https://doi.org/10.20965/jdr.2018.p0677

Paper:

Free-Flow Sediment Flushing: Insights from Prototype-Scale Studies

Taymaz Esmaeili[*,†], **Tetsuya Sumi**[**], **Sameh A. Kantoush**[**], **and Yoji Kubota**[***]

[*]Department of Civil Engineering, Gorgan Branch, Islamic Azad University
Gorgan 49147-39975, Iran
[†]Corresponding author, E-mail: taymaz.esmaeili@gmail.com, t.esmaeili@gorganiau.ac.ir
[**]Disaster Prevention Research Institute (DPRI), Kyoto University, Kyoto, Japan
[***]Hydro Technology Institute Co., Ltd., Osaka, Japan
[Received May 17, 2018; accepted June 11, 2018]

Free-flow sediment flushing operation offers viable means to preserve the storage capacity of dam reservoirs as the incoming flood erodes the flushing channel, and the deposited sediment is flushed from the reservoir. This method involves complex flow patterns and flushing channel formation procedures owing to the dynamic interaction between varying flow conditions (e.g., shallow and deep flows) and moveable bed variations notably when the non-uniform sediments exist in the complex geometry of reservoirs. In the present study, first, the numerical simulation of a previously conducted free-flow sediment flushing operation in the Dashidaira and the target segment of Unazuki reservoirs using the available field-measured data were presented. Then, to improve the flushing efficiency in the Dashidaira reservoir, the effects of using a groyne were studied. A fully 3D numerical model using the finite volume method in combination with a wetting/draying algorithm was utilized to reproduce the flow velocity field and morphological bed changes. While the characteristics of the flow field can be captured by the numerical model in Dashidaira and Unazuki reservoirs, simulated bed changes in upstream areas covered with the coarser materials (e.g., study zone of Unazuki reservoir) showed some discrepancies. The outcomes also revealed that implementing a groyne at the entrance of the wide midstream of Dashidaira reservoir can locally increase the sediment erosion chance from this area and thereby can improve the flushing efficiency by approximately 10%. Therefore, the risks associated with the accumulation of distorted sediments in the wide midstream of Dashidaira reservoir within a long-term period could be reduced.

Keywords: reservoir sediment flushing, 3D numerical model, bed changes, flushing efficiency

1. Introduction

Dams interrupt the natural sediment transportation process through rivers, which results in sediment deposition in the reservoirs behind dams [1]. According to the literature, 0.5% of the total storage volume of reservoirs is annually lost worldwide owing to the sedimentation [2]. Sedimentation negatively affects the functionality of reservoirs in terms of flood control, hydropower generation, irrigation, and drinking water supply, thereby generating substantial economic losses during their life span [1, 3, 4]. Various measures have been adopted to control the progressive deposition of sediments in reservoirs in order to prolong their lifespan, including sediment dredging, density current venting, bypassing, flushing, sluicing, and upstream sediment trapping [1, 5]. Amongst different measures for controlling progressive sedimentation in reservoirs to prolong their life, drawdown flushing (i.e., free-flow sediment flushing) has a significant contribution on storage capacity restoration and conservation since it is an efficient hydraulic technique for sediment removal [6]. This technique involves completely lowering the water level by opening the bottom outlets to establish free flow through the outlets during a specific time period. The accelerated flow scours a channel in the deposited sediments and flushes out both fine and coarse sediments [4, 5, 7]. However, only few experimental studies have focused on flushing channel formation [7], and limited research has been conducted to explain flushing channel formation and evolution in prototype reservoirs [8].

The sediment load produced by catchments in Japan is generally high due to the geologically young mountains, steep slopes, flashy flow regimes, and frequent landslides that especially occur in mountainous areas. Consequently, the amount of both sediment transported by rivers and sediment input of reservoirs located along these rivers are significantly high. Kurobe River, located in the Toyama prefecture, is one of the most important rivers in Japan because of the cascade reservoir system along this river and the remarkable amount of generated hydro-power electricity by these reservoirs. Thus, the reservoir owners are interested in implementing practically applicable mea-

sures to increase sediment removal from these reservoirs, especially from those areas that encounter excessive sediment deposition problems.

When the condition of water depth varies from shallow to deep and meanwhile sandbars exist in a reservoir, numerical models that are more sophisticated than the simple one-dimensional (i.e., 1D) models should be used to optimize the sediment management strategies in reservoirs [9]. Advanced two-dimensional (i.e., 2D) numerical models are employed to solve practical problems in rivers (e.g., simulation of morphological bed changes in river meanders); however, such 2D and also quasi three-dimensional (i.e., 3D) numerical models cannot directly simulate a complex 3D flow field that includes secondary currents whereas these currents contribute significantly to the natural sediment transport processes [10]. Thus, using the 3D numerical models is essential if the velocity variation over the flow depth, i.e., helical flow, is a dominating factor in sediment transport (e.g., in channel bends). Recently, 3D numerical models were used to investigate the sediment dynamics inside reservoirs during flushing operations at the both lab scale (e.g., [11, 12]) experiments and the full scale (e.g., [13–15]).

A software package called SSIIM (Simulation of Sediment Movements In water Intakes with Multiblock Option) has been used in this study. The SSIIM program implements a 3D numerical model of the flow field by solving the mass and momentum conservation equations in three dimensions using different turbulence models [16]. SSIIM was successfully used for coupled computation of the flow and sediment field in physical model and prototype-scale studies by various researchers [17–21]. Recently, this Computational Fluid Dynamics (CFD) program was used with enhanced grid generation features to simulate the sedimentation and flushing channel evolution in reservoirs [15, 22, 23]. Nonetheless, it is worth noting that the simulation of a sediment-flushing event in steep full-scale reservoirs, such as the Dashidaira and Unazuki reservoirs, is complex because of the rapid change in hydraulic boundary conditions and bed sediment sizes even within short distances. Furthermore, numerical studies focusing on potential measures for increasing the sediment flushing efficiency in prototype-scale reservoirs are scarce. Additionally, the increased frequency of extreme floods associated with high sediment yield in the catchment, pronounces developing efficient sediment management strategies in reservoirs (e.g., free-flow sediment flushing) to conserve the storage capacity of reservoirs and consequently mitigate sedimentation problems and reduce the risk of disasters caused by sedimentation in reservoirs.

In the present study, the SSIIM model was employed to simulate the 2012 free-flow sediment flushing operation in the both Dashidaira and Unazuki reservoirs using the field-measured data. To do this, the calibrated model of the Dashidaira reservoir through the sensitivity analysis of computed Total Volume of Flushed Sediments (i.e., TVFS) as a result of changes in the selected empirical parameters together with assessment of morphological bed changes was used. The same calibration process was also accepted for the study zone of Unazuki reservoir (i.e., upstream half of the reservoir). Because of the interest to increase the Flushing Efficiency (i.e., FE), which is defined as the ratio of flushed sediment volume to the used water volume, effect of the construction of a groyne in the entrance of wide midstream area, where encounters the excessive sediment deposition problem, were numerically summarized in the Dashidaira reservoir to investigate how this structure affect the morphological bed changes in specific zones of the reservoir and whether it can increase the FE. To provide a more detailed and quantitative insight on morphological bed changes (i.e., erosion or deposition), the Bed Changes Index (i.e., BCI) is also introduced and employed to figure out the average bed changes in each area of the study case compared to a reference case (e.g., calibrated case).

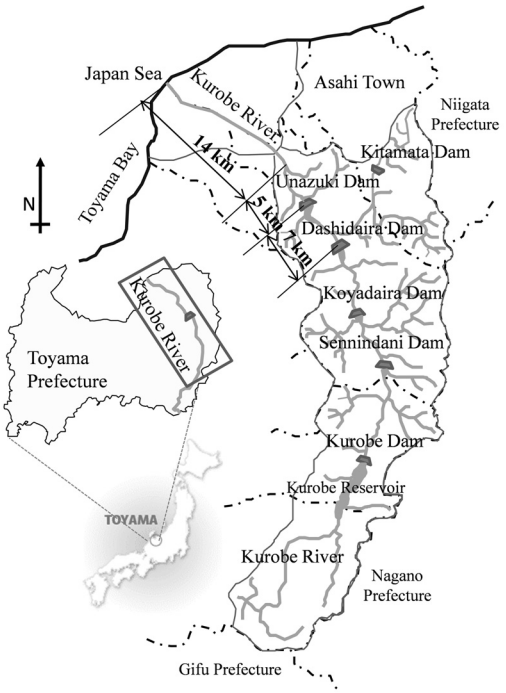

Fig. 1. Site map of the Kurobe River illustrating the location of the Dashidaira and Unazuki reservoirs [24].

2. Description of Case Studies

2.1. Sites Background

The Kurobe River originates from the Washiba Mountain with an elevation of 3000 m, located in the northern Japanese Alps, and flows into Toyama Bay in the Japan Sea (**Fig. 1**) [24]. The catchment area of the river is 682 km^2, and the length of the river is 85 km. The steep bed slope of the river varies between 1% and 20%. In the catchment area of the Kurobe River, the average rainfall and total sediment yield are 4000 mm and 1.4×10^6 m^3/year, respectively, which are both among

the highest in Japan [25]. The Dashidaira dam, with a height of 76.7 m and generating capacity of 124 MW, was constructed on the Kurobe River by the Kansai Electric Power Company in 1985. The average bed slope of the reservoir is approximately 2.2% with the gross and effective storage capacities of 9.01 and 1.66 million m^3, respectively [5, 25]. The multipurpose Unazuki gravity dam with a height of 97 m has been completed in 2000. The dam is mainly used for flood control purpose whereas water supply and power generation are other functions of the dam. A discharge of 700 m^3/s can be regulated by the dam when a flood occurs with 6900 m^3/s peak discharge. This dam has been built 7 km downstream of the Dashidaira dam with gross and effective storage capacity of 27.7 and 12.7 million m^3, respectively [24, 25]. The mean annual sediment loads of Dashidaira and Unazuki reservoirs are 0.62×10^6 m^3 and 0.96×10^6 m^3, respectively. Meanwhile the ratio of total storage to mean annual runoff in the Dashidaira and Unazuki reservoirs are 0.00674 and 0.014, respectively [26]. While Dashidaira dam is operated by Kansai Electric Power Co., Inc., Unazuki dam is controlled directly by the Ministry of Land, Infrastructure, Transport and Tourism (i.e., MLIT). Both dams are among the first dams in Japan constructed with sediment-flushing facilities. The first flushing operation in the Dashidaira reservoir was performed in 1991, 6 years after the dam construction. Consequently, the accumulated distorted sediments within 6 years were diffused to the downstream and estuary zone causing many negative environmental impacts. Since 2001, to mitigate the negative environmental impacts on the downstream areas, the coordinated sediment flushing operations are performed every year in these reservoirs during the first major flood event in the rainy season (i.e., between June and August) as the aquatic animals have adapted to the perturbation caused by natural floods. A flood not only provides enough energy to transport the flood-born sediments through the reservoir, but also scours the previously deposited sediments from the reservoir. The coordinated sediment flushing operation led to preserving the effective storage capacity of these reservoirs while reducing the environmental implications as much as possible.

2.2. Field Data Collection

The bathymetric survey to measure the bed levels is performed regularly by the reservoir owners before and after the annual coordinated sediment flushing operations in the Dashidaira and Unazuki reservoirs. The measured bed levels before the flushing operation in June 2012 and the locations of cross-sections, which were used for further assessments, are shown in **Figs. 2(a1)** and **(a2)**. The approximately 2-km length of the Dashidaira reservoir has been divided into three areas, namely, Areas I, II, and III, to analyze the study outcomes based on the generally similar types of bed materials in each area. In Area I, the bed material is coarse (e.g., gravel), while in downstream half of Area II and Area III, the bed material transitions to finer sediments (e.g., fine sand and even mud). The thalweg of the river channel exists close to the right bank of

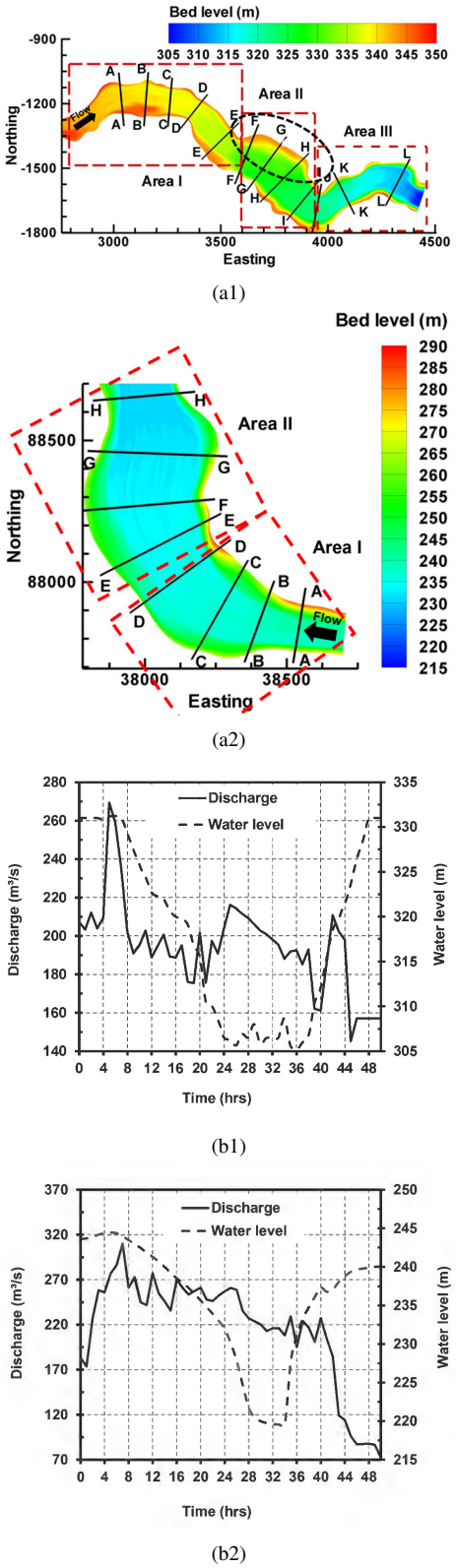

(a1)

(a2)

(b1)

(b2)

Fig. 2. Measured bed topography of (a1) Dashidaira reservoir and (a2) study zone of Unazuki reservoir before the flushing operation in June 2012 and locations of cross-sections in different areas of reservoirs; Water level and discharge rates during the flushing operation in June 2012 in (b1) Dashidaira reservoir and (b2) Unazuki reservoir.

Table 1. Average sediment size distribution in the specified cross-sections of the Dashidaira reservoir shown in **Fig. 2(a1)**. Cs. is an abbreviation for Cross-section.

Sediment Size [mm]	Cs. A-A [%]	Cs. B-B [%]	Cs. C-C [%]	Cs. D-D [%]	Cs. E-E [%]	Cs. F-F [%]	Cs. G-G [%]	Cs. H-H [%]	Cs. I-I [%]	Cs. J-J [%]	Cs. K-K [%]	Cs. L-L [%]
316	2	0	0	0	0	0	0	0	0	0	0	0
118.3	74	0	0	0	0	0	0	0	0	0	0	40
37.4	6	73	75	70	69	4	1	0	0	0	0	30
11.8	4	7	6	8	13	14	5	0	0	0	0	16
3.7	3	14	11	14	12	25	18	0	0	0	0	3
1.2	5	4	1	3	2	23	21	0	6	13	0	1
0.37	6	2	7	5	4	35	55	100	94	87	100	10

Table 2. Average sediment size distribution in the specified cross-sections of the Unazuki reservoir shown in **Fig. 2(a2)**. Cs. is an abbreviation for Cross-section.

Sediment Size [mm]	Cs. A-A [%]	Cs. B-B [%]	Cs. C-C [%]	Cs. D-D [%]	Cs. E-E [%]	Cs. F-F [%]	Cs. G-G [%]	Cs. H-H [%]
316	2	0	0	0	0	0	0	0
118.3	73	63	53	53	40	10	1	0
37.4	16	21	26	26	36	38	21	1
11.8	8	10	9	9	10	20	23	5
3.7	1	1	3	3	8	12	22	16
1.2	0	0	0	0	0	4	10	29
0.37	2	5	9	9	6	16	23	49

the wide middle area (i.e., Area II) and subsequently fine sediments deposited along the left bank, indicated with an ellipse dashed line (i.e., dead zone) in **Fig. 2(a1)**, were not removed effectively during the flushing operation. The dam owners are interested in removing the accumulated sediments from this zone by annual flushing operation to prevent the formation of consolidated and distorted fine sediments and also to keep the effective storage capacity as much as possible. As for the Unazuki reservoir, both Areas I and II have been covered with coarse materials. Besides, temporal variation of the water level and discharge magnitudes are recorded at each dam site during the flushing operations. The inflow discharge and water level fluctuations during 2012 flushing operation, in which the major sediment inflow to the Dashidaira reservoir was a wash load (i.e., transported without deposition in the reservoir), are illustrated in **Figs. 2(b1)** and **(b2)** for the Dashidaira and Unazuki reservoirs, respectively. The free-flow state occurred from 24 to 38 and 27 to 34 hours after the start of the flushing operation in Dashidaira and Unazuki reservoirs, respectively. Also, the water level drawdown from the beginning of the operation to the free-flow state was approximately 25 m in Dashidaira reservoir and 21 m in Unazuki reservoir. Based on the samples collected onsite, seven sediment sizes ranging between 316 and 0.37 mm were considered as representative grain sizes for the bed of the reservoirs. **Tables 1** and **2** show the average sediment size distribution in different cross-sections prior to the reservoirs flushing operation.

3. Numerical Model

The 3D numerical model SSIIM solves the continuity equation together with the Reynolds-averaged Navier-Stokes equations in three dimensions and uses non-orthogonal coordinates to compute the water motion for turbulent flow [16].

The finite-volume approach is applied as a discretization method to transform the partial differential equations into algebraic equations. The convection term in Navier-Stokes equation is solved using second-order upwind scheme [11, 16]. The Reynolds stress term is modeled using the standard k-ε turbulence model with constant empirical values [27].

The unknown pressure field in the Reynolds-averaged Navier-Stokes equations is calculated by employing the semi-implicit method for pressure-linked equations [28]. An implicit free-water surface algorithm was used based on the pressure gradient between a cell and the neighbor cells. Then, the free-water surface is computed using the local elevation difference between a cell and the neigh-

boring cells [15, 16].

$$\frac{\partial p}{\partial x_i} = \rho g \frac{\partial z}{\partial x_i}, \quad \ldots\ldots\ldots\ldots\ldots (1)$$

where p is the pressure, x_i is the special geometrical scale, ρ is the water density, g is the acceleration due to gravity and z is the water-level elevation.

Because the water level in all cells is unknown, an iterative method was used. Additionally, because a number of neighboring cells were used to compute the water elevation differences for each cell, different values appeared for the water elevation difference depending on the number of neighboring cells used in the computation. Therefore, a weighted average of these values was applied. The weighted average coefficient for each neighboring cell (a_i) is a function of the Froude number, flow direction, and location of neighboring cells:

$$a_i = \begin{cases} \min(2 - Fr; 1.0) & \text{for } w > -0.1 \text{ and } Fr < 2.0 \\ w^2(Fr - 1.0) & \text{for } w < -0.5 \text{ and } Fr > 2.0 \\ 0.0 \end{cases}, \quad (2)$$

with:

$$w = \frac{\vec{r} \times \vec{u}}{|\vec{r}| \times |\vec{u}|}, \quad \ldots\ldots\ldots\ldots\ldots (3)$$

where Fr is the Froude number, w is the dot product of $\vec{r}$ and $\vec{u}$, $\vec{r}$ is the direction vector pointing from the center of a cell to the center of neighboring cell aimed to consider the upstream/downstream effect and $\vec{u}$ is the velocity vector of the cell. This coefficient is then used for discretizing the following equation [15]:

$$\sum_{i=1}^{8} a_i z_p = \sum_{i=1}^{8} a_i \left(z_i + \frac{1}{\rho g}(p_p - p_i) \right), \quad \ldots\ldots (4)$$

where z_p is the water level elevation in the cell, z_i is the water level elevation in the i-th neighboring cell, p_p is the pressure in the cell and p_i is the pressure in the i-th neighboring cell.

This implicit and iterative approach is a robust and stable method that can also be used in connection with estimates of the sediment transport and morphological bed changes under unsteady flow conditions. The use of an implicit discretization scheme allows employing large time-step sizes in the model [18].

The SSIIM model uses non-orthogonal, unstructured, and adaptive grid that moves vertically with changes in the bed and free-water surface elevation. During the computations, only the water body is modeled. The water surface is recomputed after each time step, and the employed wetting/drying algorithm enables the model to have a varying number of grid cells (e.g., in the vertical and lateral directions) with respect to the water depth in the computational domain using Eq. (5) [29]. The wetting/drying algorithm causes the cells to dry up and disappear from the computational domain if the water depth is less than a user-defined lower boundary. If the water depth becomes greater than the lower boundary in the dry area, the algorithm regenerates a cell. This approach allows using a dynamic grid that can move in the lateral direction, leading to accurately modeling the changes in the bed and water level.

$$n = n_{\max} \left(\frac{depth}{depth_{\max}} \right)^p, \quad \ldots\ldots\ldots (5)$$

where n is the number of grid cells in the vertical direction, $n_{\max}$ is the maximum number of grid cells in the vertical direction, and p is a user-defined parameter for the number of grid cells.

Dirichlet boundary condition (logarithmic velocity distribution) was used for the water inflow, whereas zero-gradient boundary condition was specified for the water outflow and sediment concentration calculations. The empirical wall law introduced by Schlichting was utilized for the boundary condition at the bed and walls, where there is no water flux [16, 30]. The bed roughness in the form of dunes and ripples is also considered using an empirical formula introduced by Van Rijn, which employs the characteristics of sediment size distribution and bed form height within the computational domain [16, 31].

The sediment transport computation for simulating the morphological changes is divided into suspended sediment and bed load transport. The suspended sediment transport is calculated by solving the transient convection-diffusion equation, as follows:

$$\frac{\partial c}{\partial t} + U_j \frac{\partial c}{\partial x_j} + w \frac{\partial c}{\partial z} = \frac{\partial}{\partial x_j} \left(\Gamma_T \frac{\partial c}{\partial x_j} \right), \quad \ldots (6)$$

where U_j is the water velocity, w is the fall velocity of the sediments, c is the sediment concentration over time t and spatial geometries (i.e., x and z), and Γ_T is the turbulent diffusivity. To compute the equilibrium suspended sediment concentration in the cells close to the bed, an empirical formula developed by Van Rijn is used as the boundary condition [32]:

$$C_{bed} = 0.015 \frac{d_i}{a} \frac{\left[\frac{\tau - \tau_{c,i}}{\tau_{c,i}} \right]^{1.5}}{\left(d_i \left[\frac{(\rho_s - \rho_w) g}{\rho_w \nu^2} \right]^{\frac{1}{3}} \right)^{0.3}}, \quad \ldots (7)$$

where a is a reference level set equal to the roughness height, d_i is the diameter of the i-th fraction, ν is the kinematic viscosity, τ is the shear stress, $\tau_{c,i}$ is the critical shear stress for d_i, which was calculated from the Shield's curve, and ρ_w and ρ_s are the density of the water and sediment, respectively.

In the SSIIM model, the bed load can be simulated using the Meyer-Peter-Müller (MPM) formula [33]. The MPM formula is appropriate for steep rivers, which mainly transport coarse sediments close to the bed:

$$q_{b,i} = \frac{1}{g} \left[\frac{\rho_w g r I - 0.047 g (\rho_s - \rho_w) d_{50}}{0.25 \rho_w{}^{\frac{1}{3}} \left(\frac{\rho_s - \rho_w}{\rho_s} \right)^{\frac{2}{3}}} \right]^{\frac{3}{2}}, \quad \ldots (8)$$

where $q_{b,i}$ is the sediment transport rate for the i-th frac-

tion of the bed load per unit width, d_{50} is the characteristic sediment size (median sediment size), r is the hydraulic radius, and I is the slope of the energy line.

The model uses a reduction function of the critical shear stress for incipient motion to account for side slope effects using the formula introduced by Brooks together with a sand slide algorithm [16, 34]. This sand slide algorithm corrects the bed slope if it exceeds the defined critical angle of repose of the sediments during excessive erosion and thereby accounts for side bank erosion. In fact, the implemented sand slide algorithm acts as a limiter when erosion continues and the bed slope increases [21].

4. Numerical Simulation

4.1. Model Preparation and Calibration

The computational grid for the Dashidaira and Unazuki reservoirs was constructed based on the bathymetric surveys conducted before flushing (**Figs. 2(a1)** and **(a2)**). The mesh cell sizes in the streamwise and transversal directions were 10–20 m and 5–10 m, respectively. The bed material density was assumed to be 2650 kg/m^3. The water levels and inflow discharge fluctuations, which were employed as the hydrodynamic boundary conditions in the simulations, are shown in **Figs. 2(b1)** and **(b2)** for Dashidaira and Unazuki reservoirs, respectively. In addition, a non-uniform bed material size distribution with spatially varying fractions was introduced to the model using the seven representative sediment sizes shown in **Tables 1** and **2**. More specifically, the computational domain was divided into a number of small segments, and each segment had its own non-uniform grain size distribution.

For calibration purposes, a reference case for simulating the free-flow sediment flushing operation in the Dashidaira reservoir was first established, assuming general values for the empirical parameters in the SSIIM model. Due to the good performance of the MPM bed load sediment transport formula for flushing simulations of Alpine reservoirs revealed by Haun et al. with conditions almost similar to those of the Dashidaira reservoir (e.g., steep slopes and a wide variety of sediment size distributions) [22] and Esmaeili et al. [35], this sediment transport formula was selected to simulate the reference case and subsequently for the sensitivity analysis and model calibration.

Then, the sensitivity of the computed TVFS to changes in the empirical parameters was investigated. The computed TVFS was compared with the measured TVFS (i.e., 408.7×10^3 m^3), and if it was larger than 75% compared to the measured one, it was considered a model case for further assessment. Then, the final simulated bed topography pattern was compared, both qualitatively and quantitatively, to the actual measurements to validate the model. The qualitative assessment was performed to check whether the erosion in Area I, where the coarser sediments exist, could be captured, and the quantitative assessment was conducted to measure the deviation of the simulated bed levels from the measured ones. Therefore, the Mean Absolute Error (MAE) of simulated bed levels after the flushing operation was calculated. The model calibration process that involved the sensitivity analysis for roughness, active layer thickness, water content of the bed material, and critical angle of repose was summarized by Esmaeili et al. [36] and their values were set as 0.5 m, 1 m, 40% and 32°, respectively. Applying these values can result in achieving a reasonable TVFS and accuracy level (i.e., 313.0×10^3 m^3, and 1.8 m) in addition to satisfying the qualitative criteria for Dashidaira reservoir mentioned above. Since the Unazuki reservoir has been located downstream of the Dashidaira reservoir and the flushing operation in the Unazuki reservoir is linked to the Dashidaira reservoir, the already obtained values for main empirical parameters in the Dashidaira reservoir have been applied for developing the calibrated model in the Unazuki reservoir. In contrast to the Dashidaira reservoir with mainly the sediment erosion in the whole reservoir area, both sediment deposition and erosion occurs in the study area of the Unazuki reservoir since significant amount of the flushed out sediment from the Dashidaira reservoir comes into the Unazuki reservoir. The measurements revealed a sediment deposition volume of 1.59×10^3 m^3 in the study zone of the Unazuki reservoir while calculation showed a sediment deposition volume of 7.22×10^3 m^3 with accuracy of about 0.6 m in this zone.

4.2. Simulation of Flow Field and Morphological Bed Changes

4.2.1. Dashidaira Reservoir

Figure 3 shows the computational grid adjustment at the beginning (i.e., $t = 10$ h; **Fig. 3(a1)**) and during the free-flow conditions with a low water head in the reservoir (i.e., $t = 32$ h; **Fig. 3(a2)**), and the corresponding surface water velocity field (i.e., **Figs. 3(b1)** and **(b2)**) [36, 37]. The cells with a smaller water head than a specified value were removed from the computational domain due to the employed wetting/drying algorithm. The grid adjustment also reveals that the flow was deflected to the right-hand side of Area II during the free-flow conditions; consequently, the flushing channel location was close to the right bank. **Fig. 3(b1)** shows that a complex flow field with a strong reverse flow pattern and water stagnant zone develops in the lower half of the reservoir. This can be attributed to the complex geometry of computational domain, the variation in flow depths from shallow conditions in the upstream areas to deep conditions in the downstream areas, and the existing bed roughness of computational domain. In addition, **Fig. 3(b2)** shows the water flow concentration in the flushing channel when the reservoir water level is at its lowest level. During the free-flow condition, as shown in **Fig. 3(b2)**, the velocities rise to approximately 4.5 m/s, and supercritical flows are likely to develop in several zones of the flushing channel. However, the 3D numerical model can capture the complex

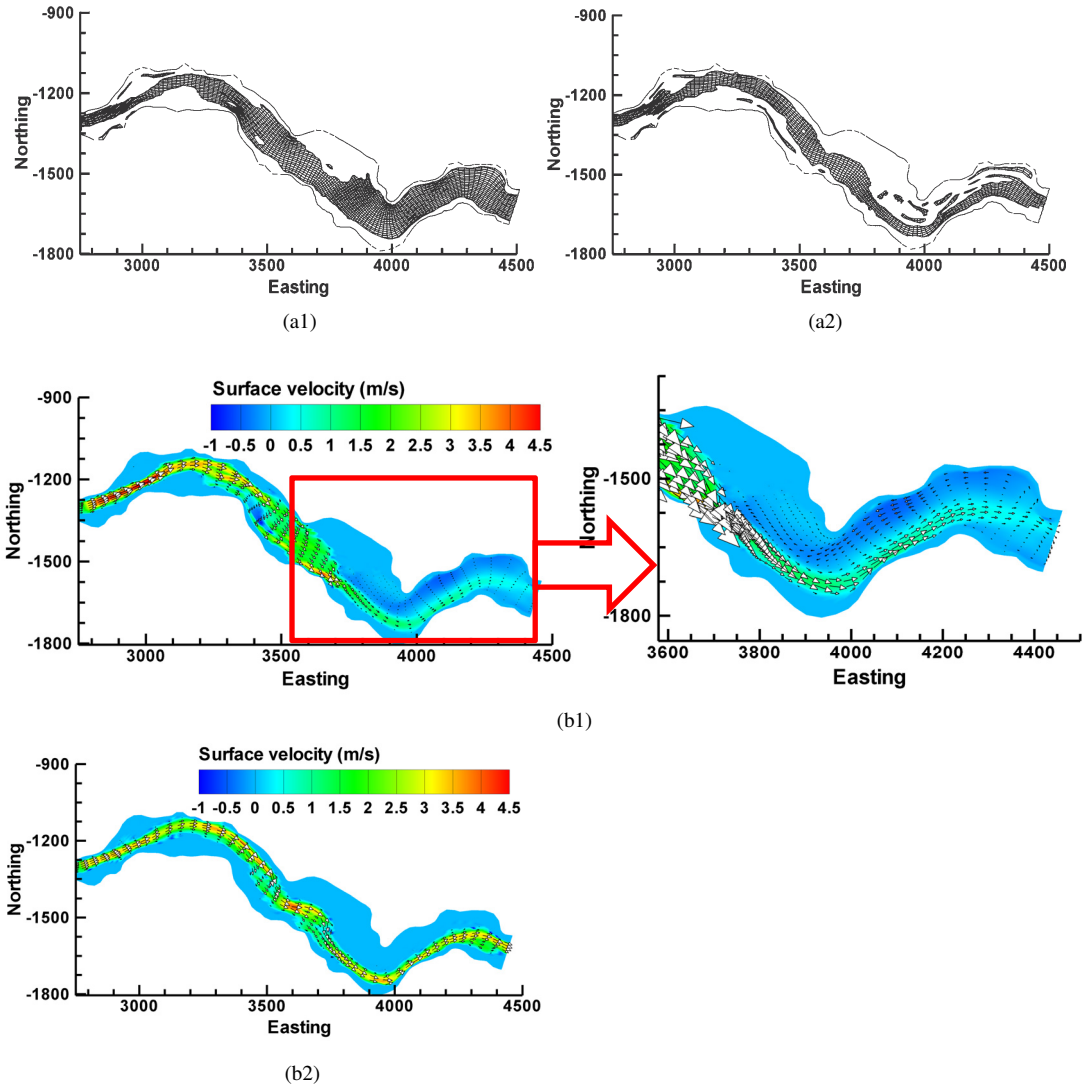

Fig. 3. Computational grid (a1) at the beginning of drawdown stage ($t = 10$ h) and (a2) during the free-flow condition in Dashidaira reservoir ($t = 32$ h); corresponding surface velocity fields: (b1) at the beginning of drawdown stage ($t = 10$ h) and (b2) during the free-flow condition ($t = 32$ h). The illustration on the right in **Fig. 2(b1)** shows the reverse flow domain and stagnant water zone [36].

characteristics of the flow field in channel bends (i.e., erosion along the outside of the bend and deposition along the inside), and the non-symmetrical velocity profile over the width as well as transverse water surface tilt at the bend apex were reproduced [35]. As can be observed from **Figs. 3(b1)** and **(b2)**, the wet areas of computational domain contain the water body and corresponding surface velocity vectors so that it is distinguished from the dry area without surface velocity vectors.

Figure 4(a) illustrates the measured bed topography after 2012 flushing operation in comparison with the simulated final bed topography after the flushing operation using MPM formula (**Fig. 4(b)**). To provide more quantitative insights into the simulated final bed topography after the flushing operation, the BCI is defined as follows [36]:

$$\mathrm{BCI} = \frac{1}{n}\sum_{i=1}^{n}\left(z_{i\_ms} - z_{i\_reference}\right), \quad \ldots\ldots \quad (9)$$

where z_{i_ms} is the measured or simulated bed level after the flushing operation at each grid node and $z_{i\_reference}$ is the measured or simulated reference bed level at the corresponding node, which is used for comparison purposes to provide information about erosion or deposition over a specific zone of the computational grid. Furthermore, n is the number of grid nodes considered for comparison purposes. Positive and negative values of BCI represent depositional and erosional conditions, respectively. In other words, BCI reveals the average change in the bed level of each target zone and readily indicates the dominant morphological process (i.e., erosion or deposition) in the zone compared to the reference case.

BCI parameter was extracted in different areas of the reservoir using the measured bed levels after flushing or simulated bed levels employing the MPM bed load sediment transport formula when the measured bed levels before flushing (**Fig. 2(a1)**) is considered as reference

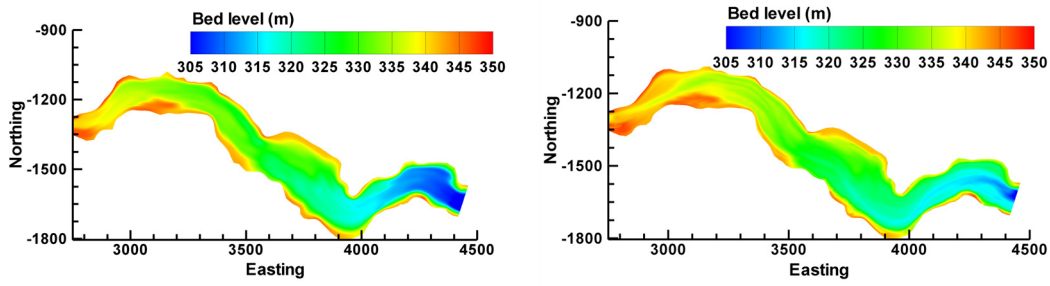

Fig. 4. (a) Plan view of the measured bed topography after the 2012 flushing operation in the Dashidaira reservoir; (b) Plan view of the simulated bed topography using the MPM formula [36].

case [36]. In the upstream area (i.e., Area I), the measurements reveal an average erosion value of 2.03, and simulated bed levels in the calibrated case show average erosion value of 1.61 m. In the wider midstream segment (i.e., Area II), the measurements using the BCI parameter reveal an average erosion value of 0.67 m whereas the simulated bed levels show an average erosion value of 1.59 m. In the area close to the dam (i.e., Area III), the simulation results show a narrower flushing channel compared to the actual measurements [36].

4.2.2. Unazuki Reservoir

Figure 5 shows the computational grid adjustment at the beginning (i.e., $t = 10$ h; **Fig. 5(a1)**), at the middle of drawdown (i.e., $t = 18$ h; **Fig. 5(a2)**), during the free-flow conditions (i.e., $t = 32$ h; **Fig. 5(a3)**), and the corresponding surface water velocity field (i.e., **Figs. 5(b1)**, **(b2)**, and **(b3)**). As shown in **Fig. 5(b1)**, at the begining of drawdown (i.e., $t = 10$ h), flushing flow deviates to the left bank of the study zone while it changes its path towards the center afterwards. This can be attributed to the complex geometry of computational domain and variation of flow depth from shallower condition in upstream segment (i.e., study zone) to deeper condition in downstream segment on the existing bed roughness. **Fig. 5(b2)** reveals the gradual shifting of flushing flow direction from left bank towards the center of the study zone. The onset of flow bifurcation and water flow concentration in two distinctive narrow flushing channels during the drawdown stage (i.e., $t = 18$ h) can also be seen in this figure. The flow bifurcation besides the water level drawdown contributes in developing two narrow channels. During the free-flow condition (i.e., $t = 32$ h), velocities increase to 2.5 m/s and super critical flows emerge in several zones of the formed flushing channels (**Fig. 5(b3)**). It should be noted that the channel transitions from the left side towards the center of reservoir and later on towards the right side, created a distributed and irregular longitudinal scouring channels in the form of small channel networks over the transition area as shown in **Fig. 6**. **Fig. 7** illustrates the measured bed changes after flushing versus the simulated one. Both the measured and numerical model results illustrate that the deposition is the dominant outcome of the flushing operations in Area I, although some erosion occurs. In this area, erosion is locally overestimated by the numerical model because of the larger size of simulated narrow and distributed channels compared to the actual measurements. In Area II, the simulation results show larger erosion magnitude than that obtain in Area I, which is consistent with the measurements. However, numerical model overestimated the erosion in this area and represented a different erosion pattern especially in the lower half of Area II. More specifically, measurements show a wide and uniform scouring channel with a thalweg located along the center of reservoir, while simulations show a wide scouring channel with a deeper part close to the right bank.

Table 3 shows the BCI parameter in the study areas using the simulated bed levels after the flushing operation compared to the BCI parameter obtained from the measured bed levels after flushing when the bed levels measured before flushing are used as the reference case. In addition, the MAE of simulated bed levels reveals larger deviation between the simulation results and actual measurements in Area I compared to Area II. This pronounces the complexity of the simulation of sediment transportation using the empirical sediment transport formulas (i.e., MPM formula) in the areas covered with the coarse materials. A very shallow flow condition also appears in the study zone, especially during the free-flow stage, which can be deflected easily due to the small disturbances as there is no a distinctive flushing channel to attract and stabilize the flow [35, 38]. However, the bed levels are not measured immediately after the flushing owing to the technical issues. As the reservoir is steep with high sediment yield and dynamic bed changes, small floods can easily disturb the morphology of river bed in the study zone. Thus, it is difficult to achieve accurate simulation results of bed changes that agree well with the actual measurements, which are not conducted immediately after the flushing operation. Nonetheless, the outcomes of the numerical model show an overall better agreement with the aerial photo taken at an early stage after the flushing operation in terms of morphological bed changes in both Areas I and II as shown in **Fig. 6**.

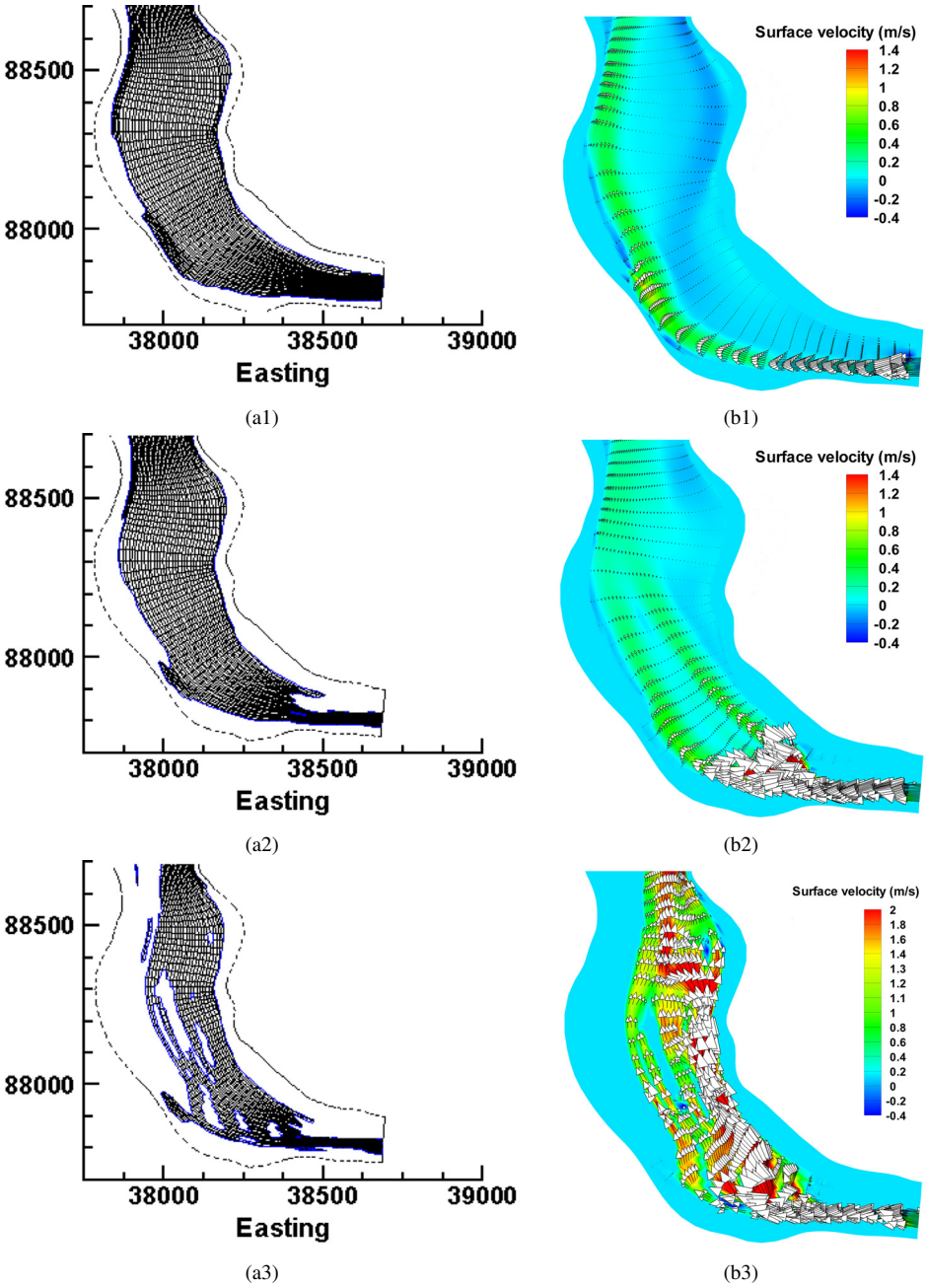

Fig. 5. Computational grid of the study zone (a1) at the beginning of simulation ($t = 10$ h), (a2) middle of drawdown ($t = 18$ h), and (a3) during the free-flow condition ($t = 32$ h) in the Unazuki reservoir; corresponding surface velocity fields: (b1) at the beginning of simulation ($t = 10$ h), (b2) middle of drawdown ($t = 18$ h), and (b3) during the free-flow condition ($t = 32$ h).

4.3. Increasing the Flushing Efficiency in Dashidaira Reservoir

Since the river thalweg exists close to the right side of the reservoir, Esmaeili et al. [36] showed that construction of an auxiliary longitudinal flushing channel in the dead zone area of Dashidaira reservoir causes a portion of the flushing flow to deviate from the main channel into the auxiliary channel and enter the main channel again via a confluence downstream of the diversion point. The non-diverted flow continues along its original path along the thalweg of main flushing channel, and the diverted flow towards the auxiliary channel scours the deposited sediments from the targeted dead zone in the reservoir. The flushing processes associated with the auxiliary longitudinal channel result in forming a longer and wider flushing channel. Therefore, FE can be increased about 9% compared to the reference case.

Another potential scenario for improving the erosion in the dead zone area of the Dashidaira reservoir is the application of a structure to alter the flow direction (i.e., groyne) at the entrance of Area II. This kind of structures can deflect a portion of the incoming flow to the left-hand side of Area II, which can scour an additional new secondary channel along the dead zone. Subse-

Fig. 6. Aerial photo showing the irrigular scouring channels after the flushing operation in the study zone of Unazuki reservoir (Photo provided by the Kurobe Office of River).

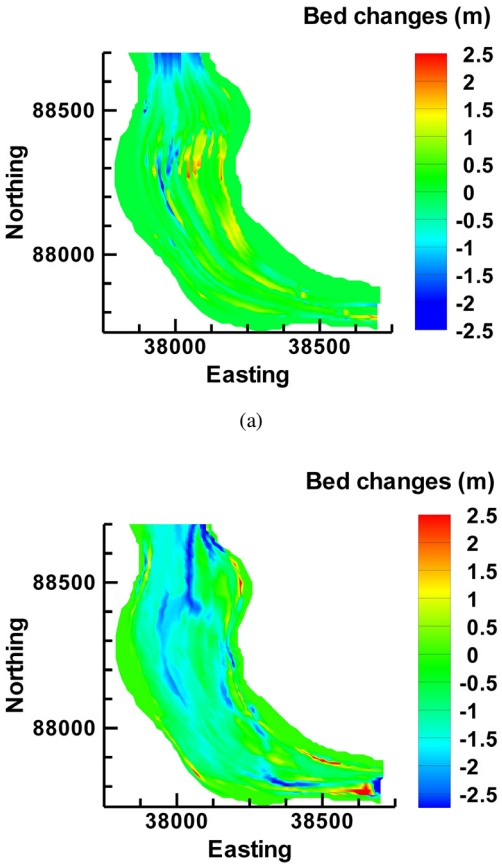

Fig. 7. (a) Plan view of the measured bed topography after 2012 flushing operation in the Unazuki reservoir; (b) Plan view of the simulated bed topography.

quently, two flushing channels will develop in Area II, the already existed one close to the right bank of Area II and another new one along the dead zone. Likewise the auxiliary longitudinal flushing channel in the dead zone area, construction of a groyne, eventually forms a finally longer and wider flushing channel resulting in higher FE. In **Fig. 8**, the surface velocity vectors before drawdown (i.e., $t = 5$ h), at the beginning of the drawdown (i.e., $t = 10$ h), in the middle of the drawdown (i.e., $t = 16$ h), and also during the free-flow condition (i.e., $t = 32$ h) were presented respectively when a groyne is used at the entrance of Area II. Before the onset of drawdown (i.e., $t = 5$ h), shown in **Fig. 8(a)**, the groyne deflects a portion of the water flow towards the left segment of Area II (i.e. dead zone), meanwhile another portion of the flow continues its original path close to the right bank of Area II because the original river thalweg exists in this area. At the beginning of the drawdown stage (i.e., $t = 10$ h), as shown in **Fig. 8(b)**, considerable amount of incoming flow is deflected towards the left-hand side of the groyne into the dead zone of Area II as a flushing channel forms in this area. During the middle of the drawdown stage (i.e., $t = 16$ h), as shown in **Fig. 8(c)**, the flow is completely divided, leading to a bifurcation of the flushing channel into two distinctive channels. In addition, a sandbar zone that formed between these channels can be clearly observed. Flow bifurcation also continues during the free-flow stage (i.e., t =32 h), as shown in **Fig. 8(d)**. **Figs. 8(c)** and **(d)** show that the head of the sandbar is eroded gradually, which causes the merging of both channels to form a wide flushing channel in the head area of sand bar. Meanwhile, the sandbar shifts further

Table 3. Average bed level changes in the study zone of the Unazuki reservoir along with the MAE of the simulated bed levels after 2012 flushing operation. The measured bed levels before the flushing used as the reference case to extract the BCI parameter.

Parameter	Measured bed level [m]		Simulated bed level [m]	
	Area I	Area II	Area I	Area II
BCI [m]	0.11	−0.07	0.11	−0.1
MAE [m]	–	–	0.62	0.52

downstream in Area II, and at the end of the free-flow stage, two distinctive flushing channels can be observed downstream of Area II. **Fig. 9(a)** illustrates the plan view of the final bed morphology after the completion of flushing operation when the groyne is used at the entrance of Area II. The two side-by-side flushing channels and their corresponding thalweg levels in Area II are apparent in this figure. Owing to the formation of an additional flushing channel along the left-hand side of Area II, the TVFS increased to reach 343×10^3 m^3 compared to the reference case value of 313×10^3 m^3. The bed levels in dif-

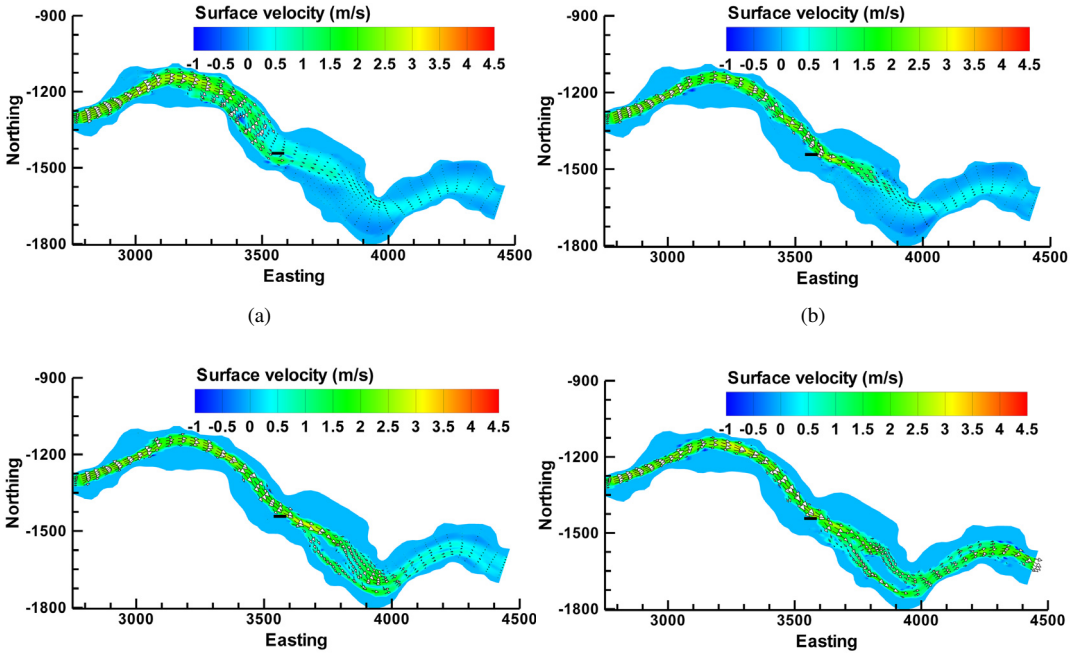

Fig. 8. Surface velocity field in different stages using a groyne in the Dashidaira reservoir: (a) before onset of drawdown stage (i.e., $t = 5$ h); (b) at the beginning of drawdown stage (i.e., $t = 10$ h); (c) at the middle of drawdown stage (i.e., $t = 16$ h); and (d) during the free-flow condition (i.e., $t = 32$ h).

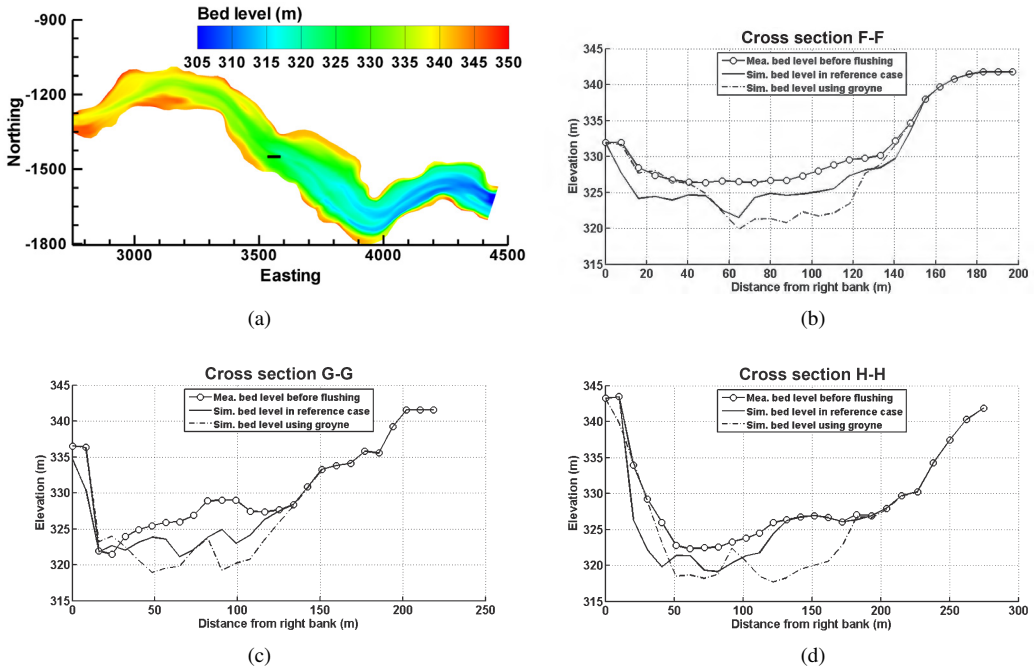

Fig. 9. (a) Plan view of the final simulated bed levels using a groyne at the entrance of Area II in the Dashidaira reservoir. Measured bed levels before flushing and simulated levels after flushing in the reference case along with simulated results using a groyne, at (b) cross section F-F; (c) cross section G-G; (d) cross section H-H. Location of the cross sections can be found in **Fig. 2(a1)**. Mea. and Sim. are abbreviations for Measured and Simulated, respectively.

ferent cross-sections of Area II when the groyne is used are shown in **Figs. 9(b)**, **(c)**, and **(d)** compared to the bed levels in the reference case.

5. Conclusion

The following outcomes were obtained from the present study:

- Building a flow guiding structure (e.g., groyne) in an appropriate location, can increase the flushing efficiency through the bifurcation of main flushing flow, thereby developing a new secondary flushing channel to scour the deposited sediments from the dead zone and merging the main and secondary flushing channel. The flushing channels are merged because of the thalweg of original flushing channel that attracts flow from the secondary flushing channel at the downstream of groyne. The flushing processes associated with the installation of a groyne result in a longer and wider flushing channel. Hence, an approximately 10% higher FE is achieved compared to the reference case.

- The study zone of Unazuki reservoir (i.e., the upstraem half) is wider with shallower flow condition compared to the other parts, especially during the free-flow stage. Furthermore, bed has not reached to equilibrium condition and there is no a distinctive flushing channel to attract and stabilize the flow in this area. Thus, flow instability takes place and flow deviates from the left to the right side of the study zone as a consequence of small disturbances during the flushing operation. This flow instability during the free flow stage causes the dynamic changes of bedtopography and formation of irregular and distributed scouring channels, which could be captured by the numerical model. The arrangement of these scouring channels cannot be observed explicitly from the bed topography measured a considerable time after flushing. Thus, it is important to measure the bed topography soon after the flushing operation to obtain a more accurate assessment of morphological bed changes caused by the flushing in the study zone.

Acknowledgements

The authors would like to give their sincere gratitude to the Kansai Electric Power Co., Inc., NEWJEC Inc., Kurobe Office of River, MLIT, and also Mr. Shuhei Minami for providing the field data used in this study.

References:

[1] G. M. Kondolf, Y. Gao, G. W. Annandale, G. L. Morris, E. Jiang, J. Zhang, Y. Cao, P. Carling, K. Fu, Q. Guo et al., "Sustainable sediment management in reservoirs and regulated rivers: Experiences from five continents," Earth's Future, Vol.2, pp. 256-280, 2014.

[2] R. White, "Evacuation of Sediments from Reservoir," Thomas Telford Publishing, 2001.

[3] G. L. Morris and J. Fan,"Reservoir Sedimentation Handbook: Design and Management of Dams, Reservoirs and Watersheds for Sustainable Use," McGraw-Hill, 1998.

[4] H. W. Shen, "Flushing sediment through reservoirs," J. Hydraul. Res., Vol.37, pp. 743-757, 1999.

[5] T. Sumi and S. A. Kantoush, "Integrated management of reservoir sediment routing by flushing, replenishing, and bypassing sediments in Japanese river basins," Proc. of the 8th Int. Symp. on Eco-hydraulics, pp. 12-16, 2010.

[6] J. Liu, S. Minami, H. Otsuki, B. Liu, and K. Ashida, "Prediction of concerted sediment flushing," J. Hydraul. Eng., Vol.130, pp.1089-1096, 2004.

[7] S. A. Kantoush, "Experimental Study on the Influence of the Geometry of Shallow Reservoirs on Flow Patterns and Sedimentation by Suspended Sediments," Ph.D. Thesis, Écolé Polytechnique Fédérale de Lausanne, 2008.

[8] C. J. Sloff, H. R. A. Jagers, and Y. Kitamura, "Study on the channel development in a wide reservoir," Proc. of the 2nd River Flow Conf., pp. 23-25, 2004.

[9] S. Fukuoka, T. Sumi, and S. Horiuchi, "Sediment management on the arase dam removal project," Proc. of the 12th Int. Symp. on River Sedimentation, pp. 1201-1209, 2013.

[10] S. Fukuoka and T. Uchida, "Toward integrated multi-scale simulations of flow and sediment transport in rivers," J. Jpn. Soc. Civ. Eng., Vol.69, pp. II_1-II_10, 2013.

[11] S. Haun and N. R. B. Olsen, "Three-dimensional numerical modelling of the flushing process of the Kali Gandaki hydropower reservoir," Lakes and Reserv., Vol.17, pp. 25-33, 2012.

[12] A. Khosronejad, C. D. Rennie, A. A. Salehi Neyshabouri, and I. Gholami, "Three-dimensional numerical modeling of reservoir sediment release," J. Hydraul. Res., Vol.46, pp. 209-223, 2008.

[13] G. Harb, C. Dorfmann, J. Schneider, and H. Badura, "Numerical analysis of sediment transport processes during a flushing event of an Alpine reservoir," Proc. of the 7th River Flow Conf., pp. 155-162, 2014.

[14] F. Gallerano and G. Cannata, "Compatibility of Reservoir Sediment Flushing and River Protection," J. Hydraul. Eng., Vol.137, pp. 1111-1125, 2011.

[15] S. Haun and N. R. B. Olsen, "Three-dimensional numerical modelling of reservoir flushing in a prototype scale," Int. J. River Basin Manag., Vol.10, pp. 341-349, 2012.

[16] N. R. B. Olsen, "A Three Dimensional Numerical Model for Simulation of Sediment Movement in Water Intakes with Multiblock Option," Department of Hydraulic and Environmental Engineering, The Norwegian University of Science and Technology: Trondheim, 2014.

[17] T. Esmaeili, T. Sumi, W. Y. Chang, and A. Vakili, "Application of steady flows for simulating the local scour depth under time varying flows," Proc. of the 12th ISRS Conf., pp. 905-912, 2013.

[18] S. Haun, H. Kjærås, S. Løvfall, and N. R. B. Olsen, "Three-dimensional measurements and numerical modelling of suspended sediments in a hydropower reservoir," J. Hydrol., Vol.479, pp. 180-188, 2013.

[19] T. Esmaeili, A. A. Dehghani, A. R. Zahiri, and K. Suzuki, "3D Numerical simulation of scouring around bridge piers (Case Study: Bridge 524 crosses the Tanana River)," World Acad. Sci. Eng. Technol., Vol.58, pp.1028-1032, 2009.

[20] T. Fischer-Antze, N. R. B. Olsen, and D. Gutknecht, "Three-dimensional CFD modeling of morphological bed changes in the Danube River," Water Resour. Res., Vol.44, 2008.

[21] N. Rüther and N. R. B. Olsen, "Modelling free-forming meander evolution in a laboratory channel using three-dimensional computational fluid dynamics," Geomorphology, Vol.89, pp. 308-319, 2007.

[22] S. Haun, C. Dorfmann, G. Harb, and N. R. B. Olsen, "Numerical modelling of the reservoir flushing of the bodendorf reservoir, Austria," 2nd IAHR European Congress, Munich, Germany, 2012.

[23] T. Esmaeili, T. Sumi, and S. A. Kantoush, "Experimental and numerical study of flushing channel formation in shallow reservoirs," J. Jpn. Soc. Civ. Eng., Vol.70, pp. I_19–I_24, 2014.

[24] S. A. Kantoush, T. Sumi, T. Suzuki, and M. Murasaki, "Impacts of sediment flushing on channel evolution and morphological processes: Case study of the Kurobe River, Japan," Proc. of the 5th River Flow Conf., pp. 1165-1173, 2010.

[25] S. Minami, K. Noguchi, H. Otsuki, H. Fukuri, N. Shimahara, J. Mizuta, and M. Takeuchi, "Coordinated sediment flushing and effect verification of fine sediment discharge operation in Kurobe River," ICOLD Conf., 2012.

[26] T. Sumi, "Evaluation of efficiency of reservoir sediment flushing in Kurobe River," Proc. of the 4th Int. Conf. on Scour and Erosion, pp. 608-613, 2008.

[27] B. E. Launder and D. B. Spalding, "Lectures in Mathematical Models of Turbulence," Academic Press, 1972.

[28] S. Patankar, "Numerical Heat Transfer and Fluid Flow," Taylor & Francis, 1980.
[29] N. R. B. Olsen and S. Haun, "Free surface algorithms for 3-D numerical modeling of flushing," Proc. of the 5th River Flow Conf., pp. 1105-1110, 2010.
[30] H. Schlichting, "Boundary Layer Theory," McGraw-Hill, 1979.
[31] L. C. Van Rijn, "Sediment transport, part III: Bed forms and alluvial roughness," J. Hydraul. Eng., Vol.110, pp. 1733-1754, 1984.
[32] L. C. Van Rijn, "Sediment transport, part II: Suspended load Transport," J. Hydraul. Eng., Vol.110, pp. 1613-1641, 1984.
[33] E. Meyer-Peter and R. Müller, "Formulas for bed load transport," 2nd Meeting of the Int. Association for Hydraulic Structures Research, IAHR, 1948.
[34] H. Brooks, "Boundary shear stress in curved trapezoidal channels," J. Hydraul. Div. Am. Soc. Civ. Eng., Vol.89, pp. 327-333, 1963.
[35] T. Esmaeili, T. Sumi, S. A. Kantoush, Y. Kubota, and S. Haun, "Numerical study on flushing channel evolution, case study of Dashidaira reservoir, Kurobe river," J. Jpn. Soc. Civ. Eng., Vol.71, pp. I_115–I_120, 2015.
[36] T. Esmaeili, T. Sumi, S. A. Kantoush, Y. Kubota, S. Haun, and N. Rüther, "Three-dimensional numerical study of free-flow sediment flushing to increase the flushing efficiency: a case-study reservoir in Japan," Water, Vol.9, p. 900, 2017.
[37] T. Sumi, S. Kantoush, T. Esmaeili, and G. Ock, "Reservoir sediment flushing and replenishment below dams: insights from Japanese case-studies," Gravel-bed rivers: processes and disasters, D. Tsutsumi and J. B. Laronne eds., John Wiley & Sons, pp. 385-414, 2017.
[38] S. A. Kantoush and A. J. Schleiss, "Channel formation in large shallow reservoirs with different geometries during flushing," J. Environ. Technol., Vol.30, pp. 855-863, 2009.

Name:
Taymaz Esmaeili

Affiliation:
Assistant Professor, Department of Civil Engineering, Faculty of Engineering, Islamic Azad University of Gorgan

Address:
Daneshjoo St., Kalantari Blvd., Gorgan 49147-39975, Iran

Brief Career:
2009-2012 Lecturer, Department of Civil Engineering, Islamic Azad University of Aq Qala
2015-present Assistant Professor, Department of Civil Engineering, Faculty of Engineering, Islamic Azad University of Gorgan

Selected Publications:
• "Three-Dimensional Numerical Study of Free-Flow Sediment Flushing to Increase the Flushing Efficiency: A Case-Study Reservoir in Japan," Water, Vol.9, No.11, 2017.
• "Experimental and Numerical Study of Flushing Channel Formation in Shallow Reservoirs," J. of Japan Society of Civil Engineers, Vol.70, No.4, pp. I_19-I_24, 2014.

Academic Societies & Scientific Organizations:
• Iranian Hydraulic Association (IHA)
• Japan Society of Civil Engineers (JSCE)

Name:
Tetsuya Sumi

Affiliation:
Director, Professor, Water Resources Research Center, Disaster Prevention Research Institute, Kyoto University

Address:
Gokasho, Uji-Shi, Kyoto 611-0011, Japan

Brief Career:
1995- Senior Research Engineer, Public Works Research Institute, Ministry of Construction
1998- Associate Professor, Department of Civil and Earth Resources Engineering, Kyoto University
2011-present Professor, Water Resources Research Center, Disaster Prevention Research Institute, Kyoto University

Selected Publications:
• "Reservoir Sediment Flushing and Replenishment Below Dams: Insights from Japanese Case Studies," Gravel-Bed Rivers: Process and Disasters, Chapter 14, D. Tsutsumi ed., ISBN: 978-1-118-97140-6 385, 2017.
• "Japan-Egypt Hydro Network: Science and Technology Collaborative Research for Flash Flood Management," J. Disaster Res., Vol.8, No.1, 2013.

Academic Societies & Scientific Organizations:
• International Association for Hydro-Environment Engineering and Research (IAHR)
• Japan Society of Civil Engineers (JSCE)
• Japan Society of Dam Engineers (JSDE)

Name:
Sameh A. Kantoush

Affiliation:
Associate Professor, Water Resources Research Center, Disaster Prevention Research Institute, Kyoto University

Address:
Gokasho, Uji-Shi, Kyoto 611-0011, Japan

Brief Career:
2003-2008 Research Assistant/Postdoctoral Research Fellow, Swiss Federal Institute of Technology at Lausanne
2011-2014 Associate Professor, Civil Engineering Department, Faculty of Engineering and Material Science, German University in Cairo
2014-present Associate Professor, Water Resources Research Center, Disaster Prevention Research Institute, Kyoto University

Selected Publications:
• "Impact of Upstream Hydropower Dams and Climate Change on Hydrodynamics of Vietnamese Mekong Delta," J. of Japan Society of Civil Engineers, Vol.73, No.4, pp. I_109-I_114, 2017.
• "The Nile Delta: Urbanizing on Diminishing Resources," J. of Built Environment, Vol.40, No.2, pp. 201-212, 2014.

Academic Societies & Scientific Organizations:
• Japan Society of Civil Engineers (JSCE)
• International Association for Hydro-Environment Engineering and Research (IAHR)
• Syndicate of Engineers, Egypt

Name:
Yoji Kubota

Affiliation:
Deputy Group Manager, River Hydraulics and Engneering Department, Hydro Technology Institute Co., Ltd.

Address:
Nakanoshima, Osaka 530-6126, Japan

Brief Career:
2005-2008 Engineer, Hydro Technology Institute Co., Ltd.
2008-2018 Project Manager, River Hydraulics and Engneering Department, Hydro Technology Institute Co., Ltd.
2018-present Deputy Group Manager, River Hydraulics and Engneering Department, Hydro Technology Institute Co., Ltd.

Selected Publications:
• "Diversion Properties Of Sediment Bypass Facilities Using Three-Dimensional Sediment Transport Model," J. of Japan Society of Civil Engineers, Vol.71, No.4, pp. I_781-I_786, 2015.
• "Impact Of The River Bed Level On Diversion Properties Of The Sediment Bypass Facility In The Koshibu Dam," J. of Japan Society of Civil Engineers, Vol.72, No.4 pp. I_679-I_684, 2016.

Academic Societies & Scientific Organizations:
• Japan Society of Civil Engineers (JSCE)